HHS Public Access

Author manuscript

Nature. Author manuscript; available in PMC 2014 March 19.

Published in final edited form as:

Nature. 2013 September 19; 501(7467): 412–415. doi:10.1038/nature12474.

Germline mtDNA mutations aggravate ageing and can impair brain development

Jaime M. Ross[1,*], **James B. Stewart**[2,*], **Erik Hagström**[3], **Stefan Brené**[4], **Arnaud Mourier**[2], **Giuseppe Coppotelli**[1], **Christoph Freyer**[2,3], **Marie Lagouge**[2], **Barry J. Hoffer**[5], **Lars Olson**[1], and **Nils-Göran Larsson**[2,3]

[1]Department of Neuroscience, Karolinska Institutet, Retzius väg 8, 171 77 Stockholm, Sweden

[2]Max Planck Institute for Biology of Ageing, Joseph-Stelzmann-Strasse 9b, 50931 Cologne, Germany

[3]Department of Laboratory Medicine, Karolinska Institutet, Retzius väg 8, 171 77 Stockholm, Sweden

[4]Department of Neurobiology, Care Sciences, and Society, KERIC, Karolinska Institutet, 171 76 Stockholm, Sweden

[5]Department of Neurosurgery, Case Western Reserve University School of Medicine, 11100 Eucid Avenue, Cleveland, OH 44106, USA

Ageing is due to accumulation of various types of damage[1,2] and mitochondrial dysfunction has for a long time been considered important[3–8]. There is substantial sequence variation in mammalian mtDNA[9] and the high mutation rate is counteracted by different mechanisms that decrease maternal transmission of mutated mtDNA[10–13]. Despite these protective mechanisms[14], it is becoming increasingly apparent that low-level mtDNA heteroplasmy is quite common and often inherited in humans[15,16]. We designed a series of mouse mutants to investigate to what extent inherited mtDNA mutations can contribute to ageing. We report that maternally transmitted mtDNA mutations can induce mild ageing phenotypes in mice with a wild-type nuclear genome. Furthermore, maternally transmitted mtDNA mutations lead to anticipation of impaired fecundity in mice that are heterozygous for the mtDNA mutator allele (*PolgA*$^{wt/mut}$) and aggravate premature ageing phenotypes in mtDNA mutator mice (*PolgA*$^{mut/mut}$). Unexpectedly, a combination of maternally transmitted and somatic mtDNA mutations also leads to stochastic brain malformations. Our findings show that a preexisting mutation load will not only allow somatic mutagenesis to create a critically high

Correspondence and requests for materials should be addressed to L.O. (lars.olson@ki.se) or N.G.L. (Larsson@age.mpg.de).

*These authors contributed equally to this work.

AUTHOR CONTRIBUTIONS

J.M.R., J.B.S. and G.C. performed breeding and phenotypic analyses of mice. J.B.S., E.H. and C.F. performed mtDNA sequence analysis. J.M.R., J.B.S. and S.B. performed histology and MRI analyses. A.M. and M.L. performed molecular analyses and measurement of respiratory chain function. J.M.R., J.B.S., B.J.H., L.O. and N.G.L conceived the ideas, designed the experiments and wrote the paper.

The authors declare no competing financial interests.

total mtDNA mutation load sooner, but will also increase clonal expansion of mtDNA mutations[17] to enhance the normally occurring mosaic respiratory chain deficiency in ageing tissues[18,19]. Our findings suggest that maternally transmitted mtDNA mutations may play a similar role in aggravating aspects of normal human ageing.

We generated a series of inbred mutant mice (Fig. 1a–c) to study the role of mtDNA mutations in ageing, taking into account that *PolgA*$^{wt/mut}$ mice transmit low levels of mtDNA mutations through the germline[20]. A standard intercross of *PolgA*$^{wt/mut}$ mice (Fig. 1a) was used to generate: *Type I mice* = mice with a wild-type nuclear genome (*wt*^{N}) containing maternally transmitted mtDNA mutations, *Type II mice* = *PolgA*$^{wt/mut}$ mice containing maternally transmitted mtDNA mutations, and *Type III mice* = *PolgA*$^{mut/mut}$ mice[21,22] containing maternally transmitted mtDNA mutations. In addition, we crossed *PolgA*$^{wt/mut}$ males to wild-type females (Fig. 1b) to generate: *Type IV mice* = *wt*^{N} mice lacking maternally transmitted mtDNA mutations and *Type V mice* = *PolgA*$^{wt/mut}$ mice lacking maternally transmitted mtDNA mutations. Finally, we crossed *PolgA*$^{wt/mut}$ males with females that have a heterozygous knockout for the catalytic subunit of mitochondrial DNA polymerase[23] (*PolgA*$^{wt/KO}$) (Fig. 1c) to generate: *Type VI mice* = a variant of mtDNA mutator mice (genotype *PolgA*$^{KO/mut}$) lacking maternally transmitted mtDNA mutations. Next, we quantitatively assessed mtDNA mutation loads and found that *Type I-III* mice contained an excess of recurring mtDNA mutations ($p<0.0001$, Fisher's exact test) (Supplementary Fig. 1a,b and Supplementary Table 1) undergoing clonal expansion (Supplementary Table 2). The PCR, cloning, and sequencing protocol has, on theoretical grounds, been criticized for artificially inducing mtDNA mutations[24,25]. We therefore used an independent method, λ-phage cloning of full-length mtDNA[20], to analyze *Type I, II, III* and *V* mice and found that the mtDNA mutation levels were very similar with both methods (Supplementary Fig. 1a,c and Supplementary Table 1), demonstrating that artificial mutations are not induced by the PCR, cloning, and sequencing protocol.

Continuous intercrosses of *PolgA*$^{wt/mut}$ animals to generate *PolgA*$^{mut/mut}$ mice (Fig. 1a) produce low litter sizes (Fig. 2a, black bars), low total number of litters per female (Fig. 2b, black bars), and less than mendelian proportions of mtDNA mutator mice (Fig. 2c, black bars). We re-introduced wild-type mtDNA into *PolgA*$^{wt/mut}$ females and a subsequent intercross gave larger litter sizes (Fig. 2a, red bar), higher number of litters per female (Fig. 2b, red bar) and a high proportion of born *PolgA*$^{mut/mut}$ mice (Fig. 2c, red bar). The reciprocal experiment, wherein wild-type males were crossed with *PolgA*$^{wt/mut}$ females to obtain *PolgA*$^{wt/mut}$ animals for subsequent intercrossing showed no improvement of fertility phenotypes (Fig. 2a–c, grey bars). Next, we decided to continue intercrossing *PolgA*$^{wt/mut}$ animals for several generations without additional re-introductions of wild-type mtDNA and found a continuous decline of litter sizes (Fig. 2d, red line), number of litters per female (Fig. 2e, red line), and the proportion of *PolgA*$^{mut/mut}$ mice born (Fig. 2f, red line). The reciprocal experiment wherein wild-type males were crossed with *PolgA*$^{wt/mut}$ females to obtain *PolgA*$^{wt/mut}$ animals for subsequent intercrossing did not modify the markedly impaired fecundity (Fig. 2d–f, grey bars). Ongoing mtDNA mutagenesis in the maternal germline thus causes anticipation of fecundity phenotypes and this deterioration can be reversed by introduction of wild-type mtDNA into females.

We proceeded to study to what extent a burst of mutagenesis in the maternal germline would result in mtDNA mutation transmission to subsequent generations. To this end, we bred *PolgA*$^{wt/mut}$ females with re-introduced wild-type mtDNA (n=8) to wild-type males (Supplementary Fig. 2a) and followed segregation of mutated mtDNA in *wt*^{N} maternal lineages (n=13). Sequencing showed that heteroplasmic mtDNA mutations were present in all *wt*^{N} mice in generation N2-N8 (n=387 individuals). In total, 192 different clonally expanded mtDNA mutations were identified (Supplementary Fig. 2b).

Next, we generated three different types of *wt*^{N} mice: *wt*^{N}*−1* = *wt*^{N} mice obtained from a standard *PolgA*$^{wt/mut}$ intercross (Fig. 1a), *wt*^{N}*−2* = *wt*^{N} mice obtained from a *PolgA*$^{wt/mut}$ intercross where the female contains re-introduced mtDNA (Fig. 1b) and *wt*^{N}*−3* = *wt*^{N} mice obtained from a *PolgA*$^{wt/mut}$ intercross where the male contains re-introduced mtDNA. The *wt*^{N}*−1* mice had significantly lower body weight than *wt*^{N}*−2* mice (Fig. 3a), whereas there was a similar reduction in body weight in *wt*^{N}*−1* and *wt*^{N}*−3* mice (Supplementary Fig. 3a). The body weights of *wt*^{N}*−2* mice decreased as crosses were continued without re-introduction of wild-type mtDNA (Fig. 3a). At 65 weeks of age, *wt*^{N}*−1* mice showed a significant ageing-associated phenotype (mean score = 2.5; SD = 1.8), whereas *wt*^{N}*−2* mice demonstrated virtually no such phenotypes (mean score = 0.16, SD = 0.2, p = 0.008) (Fig. 3b). The score increased in successive generations of *wt*^{N}*−2* mice (Fig. 3b) and was elevated to a similar extent in *wt*^{N}*−1* and *wt*^{N}*−3* mice (Supplementary Fig. 3b). We also analyzed behavior and found that spontaneous rearing was higher in *wt*^{N}*−2* than in *wt*^{N}*−1* mice (p = 0.03) and that it decreased in successive generations of *wt*^{N}*−2* mice (p = 0.003) (Supplementary Fig. 3c). There was no difference in rearing between *wt*^{N}*−1* and *wt*^{N}*−3* mice (Supplementary Fig. 3d), whereas we found impaired rearing in 2 year-old *wt*^{N}*−1* mice in comparison with 2.3 year-old C57Bl/6N mice (p = 0.009) (Supplementary Fig. 3e). These results prompted us to analyze mtDNA mutation levels and we found that the total mutation loads and the proportion of recurring mutations increased in *wt*^{N}*−2* animals between intercross generation 1 (G1) and G4 (Fig. 3c,d and Supplementary Table 1).

We observed that *PolgA*$^{mut/mut}$ mice derived from the standard breeding had a mean life span of 42.7 weeks (n=19) (Fig. 3e, black line), as previously reported[21], whereas *PolgA*$^{mut/mut}$ mice, whose *PolgA*$^{wt/mut}$ mothers lacked maternally transmitted mtDNA mutations, had a mean life span of 50.2 weeks (n=26) (Fig. 3e, red line). This increase in life span was statistically significant (p<0.0001) and was completely reversed in *PolgA*$^{mut/mut}$ mice born to *PolgA*$^{wt/mut}$ mothers maintained by intercrossing for several generations after re-introduction of wild-type mtDNA (mean life span ~43.5 weeks, n=13) (Fig. 3e, grey line).

Detailed phenotyping was performed for mtDNA mutator mice of *Type III* and *VI* at age ~35 weeks and revealed a comparable reduction in body mass (Supplementary Fig. 4a). The reduction in hemoglobin concentration (Supplementary Fig. 4b), the reduction in erythrocyte count (Supplementary Fig. 4b) and the degree of compensatory splenomegaly (Supplementary Fig. 4c) were almost identical, indicating a similar reduction of hematopoietic stem cell capacity in both types of mice. The ratio of heart weight to body weight was increased in both mouse types (p<0.0001, ANOVA) (Fig. 3f), consistent with cardiomyopathy development[21]. However, the hearts from *Type III* mice were more

enlarged than those from *Type VI* mice (Fig. 3f; p=0.023, 2-tailed t-test, Welch's Correction). Consistently, the complex IV (cytochrome c oxidase, COX) activity was reduced in *Type III*, but not in *Type VI* mice (Fig. 3g). Clonally expanded mtDNA mutations typically create a mosaic pattern of respiratory chain deficient cells in the colon of mice and humans[26,27] and such COX-deficient colonic crypts were abundant in both *Type III* and *VI* mice (Fig. 3h and Supplementary Fig. 4e). However, the proportion of COX-deficient colonic crypts was significantly higher in *Type III* than *Type VI* mice (Fig. 3h), indicating increased levels of clonally expanded mtDNA mutations. We assessed male fertility and found that *Type III* mice were sterile (Fig. 3i), as previously reported[21], whereas *Type VI* males were fertile and could produce offspring, albeit with reduced litter sizes (mean=4.3±2.2) in comparison with controls (7.2±2.6 pups per litter) (Fig. 3i). These findings show that the ongoing massive somatic mutagenesis of mtDNA is sufficient on its own to drive the hematological stem cell phenotype[28–30], whereas maternally transmitted mtDNA mutations contribute to phenotypes in other rapidly proliferating tissues, such as testis and colon, and in postmitotic tissues, such as heart, of mtDNA mutator mice[21,22].

Unexpectedly, when performing MRI studies of ageing phenotypes, we found a gross brain malformation in an mtDNA mutator mouse (Fig. 4a), which, on subsequent histology, was shown to be due to mosaic subcortical and striatal perturbations, as well as malformations affecting both the right and left hippocampus (Fig. 4b). Succinate dehydrogenase enzyme histochemistry of the same brain revealed areas of increased activity (Fig. 4c), suggesting increased cell density and/or compensatory mitochondrial biogenesis. Based on this observation, we performed a systematic study of brain morphology in mtDNA mutator mice from the standard breeding (*Type III* mice). Microscopic, and occasionally also macroscopic, brain malformations were observed in ~32% of the mtDNA mutator mice (n=13 of 41 mice), but not in wild-type mice (n=0 of 46 mice) at ages 7–46 weeks. Brain malformations were equally common in both sexes (41.5% female and 58.5% male) and most malformations were focal (69%) and manifested as different forms of brain asymmetries (Fig. 4a–c). Some mtDNA mutator mice (n=4) had widespread bilateral brain malformations, which included cortical and hippocampal lamination disturbances, hypertrophic/hyperplastic changes in hippocampus and cerebral cortex and hyperplasia in cerebellum (Fig. 4d–f). Brain malformations were not observed in *Type I* or *II* mice, despite that they contain maternally transmitted mtDNA mutations, or in mtDNA mutator mice (n=11) born to PolgA$^{wt/mut}$ mothers with re-introduced wild-type mtDNA. These findings strongly suggest that a dual hit, i.e. the presence of maternally inherited mtDNA mutations in combination with massive somatic mutagenesis of mtDNA, is required for brain malformations to occur.

To summarize, our findings show that maternally transmitted mtDNA mutations provide a baseline mutation load upon which somatic mutagenesis will act. We show that low levels of germline-transmitted mtDNA mutations *per se* can have life-long consequences and cause premature ageing. We also show that germline-transmitted mtDNA mutations constitute a risk factor that may lead to developmental disturbances if combined with increased somatic mutagenesis of mtDNA. These findings suggest that inherited human mtDNA sequence

variation and low level heteroplasmy combined with somatic mtDNA mutagenesis may have an additive effect in creating phenotypes relevant for human pathology and ageing.

METHODS SUMMARY

Mice expressing the exonuclease-deficient mitochondrial DNA polymerase gamma were maintained on the inbred C57Bl/6NCrl background. The study was performed in strict accordance with guidelines of the Federation of the European Laboratory Animal Science Association. Protocols were approved by the Landesamt für Natur, Umwelt und Verbraucherschutz, Nordrhein-Westfalen, Germany and the animal welfare ethics committee in Sweden. Complete mtDNA sequencing was carried out as described[11], with a modified primer set (Supplementary Table 3). Mutation loads were analysed by the cloning of mtDNA fragments amplified with a high-fidelity polymerase, and individual clones were sequenced. Data were filtered against nuclear pseudogene sequences of mitochondrial origin. The data were confirmed by direct sequencing of λ-phage cloned complete mtDNAs, and clonal expansion was confirmed by quantitative RFLP-PCR analyses. Blood analyses were performed by Laboklin GMBH & CO. KG (Bad Kissingen, DE). Clonal expansion analysis of mouse colonic tissues was performed as described[26,27]. Brain morphology was analysed by MRI with a BioSpec Avance 47/40 (Bruker, Ettlingen, Germany) or by histochemistry of brain sections stained with either cresyl violet or hematoxylin and eosin.

METHODS

Animals

All of the mice in this study were on an inbred C57Bl/6NCrl nuclear background. The study was performed in strict accordance with the recommendations and guideline of the Federation of the European Laboratory Animal Science Association (FELASA). Protocols were approved by the Landesamt für Natur, Umwelt und Verbraucherschutz, Nordrhein-Westphalen, Germany and, in Sweden, the animal welfare ethics committee and performed in accordance with Swedish law.

Complete mtDNA sequencing

The protocol used is modified slightly from that described previously[11]. Total DNA from tail biopsies from 3 week-old animals was collected, and the mitochondrial genome was amplified with a modified primer set, producing 30 overlapping fragments of 1–1.5kb (Supplementary Table 3). Each primer was tagged with M13F or M13R sequence for use in sequencing reactions[11]. Sequences were aligned to the C57Bl/6NCrl mtDNA reference sequence (JF286601.1) to detect mutations, with position numbering altered to remain consistent with the C57Bl/6J mtDNA reference sequence (NC_005089.1). Only mutations >20% in relative abundance will be detected by this assay[31], thus we excluded N1 animals (maximum mutation levels 15%) from this assay.

Mutation load analysis

A PCR-Clone-Sequence method was used to assay mutation loads. Total DNA was extracted from tail biopsy samples obtained from the mice at weaning (~3 weeks of age).

Detailed protocols have been published elsewhere[32]. Two pseudogenes of target region are found in the nuclear genome, but differ from the reference sequence by 19–20 sites. Any sequence sharing 2 or more consecutive SNPs with these pseudogenes was excluded from the analysis. An error-rate assessment of the method is described in[32]. One SNP variation was observed in 295 clones assayed, giving an observed error rate of 3.48×10^{-6}. This is less than 1/6 the mean rate observed for the wildtype C57Bl/6N. We obtained 3.3 Mb of mtDNA sequence (mean coverage = 88.7 kb/animal from an average of 91 clones per animal) from *Type I-VI* mice (Fig. 1a–c).

Lambda clones of intact mtDNA molecules were obtained as described[20]. Mitochondrial DNA was sucrose purified from livers from 10 weeks old animals to obtain sufficient mtDNA for cloning. Approximately 30 clones were chosen at random for complete mtDNA sequencing, as described above. 250,298 bp and 259,858 bp of cloned mtDNA was sequenced from two C57Bl/6N controls and showed no mtDNA mutations (error rate < 3.85×10^{-6} mut/bp at 16x sequencing depth). In total, 350 complete mtDNA molecules, corresponding to a total 5.6 Mb of mtDNA, were sequenced.

PCR-RFLP assay

Mutation level quantification by PCR-RFLP was carried out as described[13]. 1μl of lysate was used for PCR. Primers used; 5247a>G, **TGTAAAACGACGGCCAGT**AGACCTCAACTAGATTGGCAG & **CAGGAAACAGCTATGACC**GGTGACTGGCTGAGTAAGCATTAGACTG, 5839t>C and 5840g>A CCCACCTCTAGCCGGAAATCTAGC **CAGGAAACAGCTATGACC**AATGCCTGCGGCTAGCACTG). M13 tag sequences are in bold. FAM labeled primers M13F (for 5247a>G) and M13R (for 5839t>C and 5840g>A) were used for fragment detection. Restriction enzymes used in the assay were HphI for 5247a>G and NlaIII for 5839t>>C and 5840g>A, (NewEngland Biolabs).

Statistical analysis

Statistical analyses were performed using GraphPad Prizm (GraphPad Software Inc, San Diego, CA), with α=0.05.

Mitochondrial respiratory chain complex activities

Analysis of isolated respiratory chain complex activities were assayed as described[13].

Histology and enzyme histochemistry

For visualization of brain morphology, slides were stained with either cresyl violet or hematoxylin and eosin, dehydrated in increasing concentrations of ethanol (70%, 95%, and 99.5%), mounted (Entellan, VWR International AB, Stockholm, Sweden), and coverslipped. The activity of succinate dehydrogenase was visualized as previously described[33].

Tissue preparation for cryosectioning

Fresh frozen brain sections for histochemistry and in situ hybridization were prepared as described[33]. Combined cytochrome c oxidase and succinate dehydrogenase (COX-SDH)

staining of mouse colons was conducted as described[26]. Counts of colonic crypts with and without COX activity were performed by a researcher blinded to animal genotype.

Nurr1 gene expression

High stringency radioactive *in situ* hybridization was performed as previously described[33] to detect Nurr1 mRNA transcripts using a synthetic DNA oligonucleotide probe (5′-GCGTAGTGGCCACGTAGTTCTGGTGGAAGTTCTGAAGGGAGCCCGGATCG-3′; Thermo Scientific, Ulm, Germany).

Magnetic resonance imaging

Magnetic resonance imaging (MRI) was performed on animals as previously described[33] using a horizontal 4.7 T/40 cm magnet (BioSpec Avance 47/40, Bruker, Ettlingen, Germany), fitted with a 12 cm inner diameter self-shielded gradient system (max. gradient strength 200 mTm-1). A linear birdcage resonator (25 mm inner diameter) was used for excitation and detection. The sequence used for inversion recovery imaging had the following parameters: echo time (TE) 35.6 ms, repetition time (TR) 2566.8 ms, rapid acquisition with relaxation enhancement (RARE)-factor 8 with RARE-maximum 4, inversion time 450 ms, and matrix size 64 × 64 × 128 with 2 averages. The field of view (FOV) was 0.9 × 1.2 (or 1.4 for larger voxel) × 1.8 cm, yielding the following directional resolutions: 0.14 mm (dorso-lateral), 0.18 mm (left-right), and 0.14 mm (rostro-caudal).

Male Fertility Analysis

Type III males (n=8) and *Type VI* males (n=8) (Fig. 1a,c) were mated to single C57Bl/6N females. The size of the first litter was recorded. Males were removed from females after 60 days of unproductive mating, with females observed for three additional weeks to confirm that the mating was unproductive.

Rearing behavior

Spontaneous rearing activity in an open field was studied in wild-type mice derived from various crossings. A multi-cage infrared-sensitive motion detection system (Accuscan Instruments, Columbus, Ohio, USA) was used. Total rearing was recorded at 5 minute intervals over 90 minutes, and was determined by vertical sensor beam-breaks using appropriate software (VersaMax activity monitor, Accuscan Instruments). Animals were habituated in a dimly lit, low-noise, and ventilated experimental room kept at 20–22° C for one hour prior to testing. Experiments were performed between 11 am and 6 pm (light phase**).**

Phenotype scoring

The presence of alopecia, graying of the hair, body size reduction, and kyphosis were each scored on a scale of 0–3 (0, absence of phenotype; 1, moderate presence of phenotype; 2, strong presence of phenotype; 3, severe presence of phenotype) and the scores were summed for each animal. A summed score of 0 thus indicates normal ageing, whereas a score of 12 indicates marked premature ageing similar to the end-stage phenotype of mtDNA mutator mice. The animals were scored blind without knowledge of the genotype.

Supplementary Material

Refer to Web version on PubMed Central for supplementary material.

Acknowledgments

The study was supported by ERC Advanced Investigator grants (N.G.L and L.O), the Swedish Research Council (K2011-62X-21870-01-6 to N.G.L. and K2012-62X-03185-42-4 to L.O.), the Swedish Brain Foundation (N.G.L., L.O and J.M.R.), Swedish Brain Power (L.O and J.M.R.), the Parkinson Foundation in Sweden (N.G.L.), the Karolinska Distinguished Professor Award (L.O.), the Swedish Alzheimer Foundation (L.O.) the National Institutes of Health (AG04418 to L.O. and NS070825 to B.J.H.), the National Institute on Drug Abuse (J.M.R), the National Institutes of Health/Karolinska Institutet Graduate Partnerships Program (J.M.R) and the Swedish Society for Medical Research (G.C.). J.B.S acknowledges support from the United Mitochondrial Disease Foundation.

References

1. Szilard L. On the nature of the aging process. Proc Natl Acad Sci USA. 1959; 45:30–45. [PubMed: 16590351]
2. Kirkwood TBL. Understanding the odd science of aging. Cell. 2005; 120:437–447. [PubMed: 15734677]
3. Ernster L, Löw H, Nordenbrand K, Ernster B. A component promoting oxidative phosphorylation, released from mitochondria during aging. Exp Cell Res. 1955; 9:348–349. [PubMed: 13262047]
4. Miquel J, Economos AC, Fleming J, Johnson JE. Mitochondrial role in cell aging. Exp Gerontology. 1980; 15:575–591.
5. Pikó L, Hougham AJ, Bulpitt KJ. Studies of sequence heterogeneity of mitochondrial DNA from rat and mouse tissues: evidence for an increased frequency of deletions/additions with aging. Mech Ageing Dev. 1988; 43:279–293. [PubMed: 2849701]
6. Müller-Höcker J. Cytochrome-c-oxidase deficient cardiomyocytes in the human heart — An age-related phenomenon. Am J Pathol. 1989; 134:1167–1173. [PubMed: 2541614]
7. Cortopassi GA, Arnheim N. Detection of a specific mitochondrial DNA deletion in tissues of older humans. Nucleic Acids Res. 1990; 18:6927–6933. [PubMed: 2263455]
8. Corral-Debrinski M, et al. Mitochondrial DNA deletions in human brain: regional variability and increase with advanced age. Nat Genet. 1992; 2:324–329. [PubMed: 1303288]
9. Pakendorf B, Stoneking M. Mitochondrial DNA and human evolution. Annu Rev Genomics Hum Genet. 2005; 6:165–183. [PubMed: 16124858]
10. Krakauer DC, Mira A. Mitochondria and germ-cell death. Nature. 1999; 400:125–126. [PubMed: 10408437]
11. Stewart JB, et al. Strong purifying selection in transmission of mammalian mitochondrial DNA. PLoS Biol. 2008; 6:e10. [PubMed: 18232733]
12. Fan W, et al. A mouse model of mitochondrial disease reveals germline selection against severe mtDNA mutations. Science. 2008; 319:958–962. [PubMed: 18276892]
13. Freyer C, et al. Variation in germline mtDNA heteroplasmy is determined prenatally but modified during subsequent transmission. Nat Genet. 2012; 44:1282–1285. [PubMed: 23042113]
14. Stewart JB, Freyer C, Elson JL, Larsson NG. Purifying selection of mtDNA and its implications for understanding evolution and mitochondrial disease. Nat Rev Genet. 2008; 9:657–662. [PubMed: 18695671]
15. Li M, et al. Detecting heteroplasmy from high-throughput sequencing of complete human mitochondrial DNA genomes. Am J Hum Genet. 2010; 87:237–249. [PubMed: 20696290]
16. Payne BAI, et al. Universal heteroplasmy of human mitochondrial DNA. Hum Mol Genet. 2013; 22:384–390. [PubMed: 23077218]
17. Payne BAI, et al. Mitochondrial aging is accelerated by anti-retroviral therapy through the clonal expansion of mtDNA mutations. Nat Genet. 2011; 43:806–810. [PubMed: 21706004]
18. Greaves L, Turnbull D. Mitochondrial DNA mutations and ageing. Biochim Biophys Acta. 2009; 1790:1015–1020. [PubMed: 19409965]

19. Larsson NG. Somatic mitochondrial DNA mutations in mammalian aging. Annu Rev Biochem. 2010; 79:683–706. [PubMed: 20350166]
20. Ameur A, et al. Ultra-deep sequencing of mouse mitochondrial DNA: Mutational patterns and their origins. PLoS Genet. 2011; 7:e1002028. [PubMed: 21455489]
21. Trifunovic A, et al. Premature ageing in mice expressing defective mitochondrial DNA polymerase. Nature. 2004; 429:417–423. [PubMed: 15164064]
22. Kujoth GC, et al. Mitochondrial DNA mutations, oxidative stress, and apoptosis in mammalian aging. Science. 2005; 309:481–484. [PubMed: 16020738]
23. Hance N, Ekstrand MI, Trifunovic A. Mitochondrial DNA polymerase gamma is essential for mammalian embryogenesis. Hum Mol Genet. 2005; 14:1775–1783. [PubMed: 15888483]
24. Kraytsberg Y, Khrapko K, Single-molecule PCR. an artifact-free PCR approach for the analysis of somatic mutations. Expert Rev Mol Diagn. 2005; 5:809–815. [PubMed: 16149882]
25. Greaves LC, et al. Quantification of mitochondrial DNA mutation load. Aging Cell. 2009; 8:566–572. [PubMed: 19624578]
26. Greaves LC, Elson JL, Nooteboom M, Grady JP. Comparison of mitochondrial mutation spectra in ageing human colonic epithelium and disease: Absence of evidence for purifying selection in somatic mitochondrial DNA point mutations. PLoS Genet. 2012; 8:e1003082. [PubMed: 23166522]
27. Taylor RW, et al. Mitochondrial DNA mutations in human colonic crypt stem cells. J Clin Invest. 2003; 112:1351–1360. [PubMed: 14597761]
28. Ahlqvist KJ, et al. Somatic progenitor cell vulnerability to mitochondrial DNA mutagenesis underlies progeroid phenotypes in Polg mutator mice. Cell Metab. 2012; 15:100–109. [PubMed: 22225879]
29. Norddahl GL, et al. Accumulating mitochondrial DNA mutations drive premature hematopoietic aging phenotypes distinct from physiological stem cell aging. Stem Cell. 2011; 8:499–510.
30. Chen ML, et al. Erythroid dysplasia, megaloblastic anemia, and impaired lymphopoiesis arising from mitochondrial dysfunction. Blood. 2009; 114:4045–4053. [PubMed: 19734452]
31. Hancock DK, Tully LA, Levin BC. A Standard Reference Material to determine the sensitivity of techniques for detecting low-frequency mutations, SNPs, and heteroplasmies in mitochondrial DNA. Genomics. 2005; 86:446–461. [PubMed: 16024219]
32. Wanrooij S, et al. In vivo mutagenesis reveals that OriL is essential for mitochondrial DNA replication. EMBO Reports. 2012; 13:1130–1137. [PubMed: 23090476]
33. Ross JM, et al. High brain lactate is a hallmark of aging and caused by a shift in the lactate dehydrogenase A/B ratio. Proc Natl Acad Sci USA. 2010; 107:20087–20092. [PubMed: 21041631]

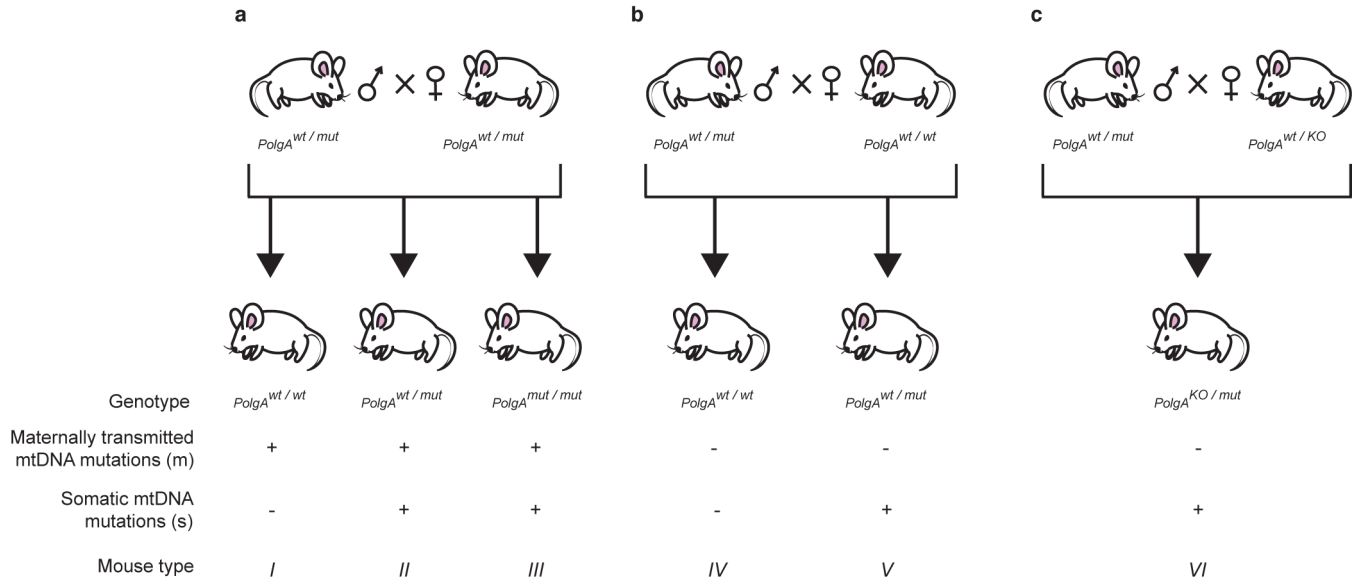

Figure 1. Breeding to generate mice with different combinations of maternally inherited and somatic mtDNA mutations

a, Intercrossing of mice heterozygous for the mtDNA mutator allele (*PolgA*$^{wt/mut}$) generates *Type I-III* mice, which inherit mtDNA mutations from their *PolgA*$^{wt/mut}$ mother. **b**, Crossing of *PolgA*$^{wt/mut}$ males and wild-type females will generate *Type IV-V* mice that lack maternally transmitted mtDNA mutations. **c**, Crossing of *PolgA*$^{wt/mut}$ males and heterozygous *PolgA* knockout females (*PolgA*$^{wt/KO}$) will generate *Type VI* mice that are an mtDNA mutator mouse variant lacking maternally inherited mtDNA mutations.

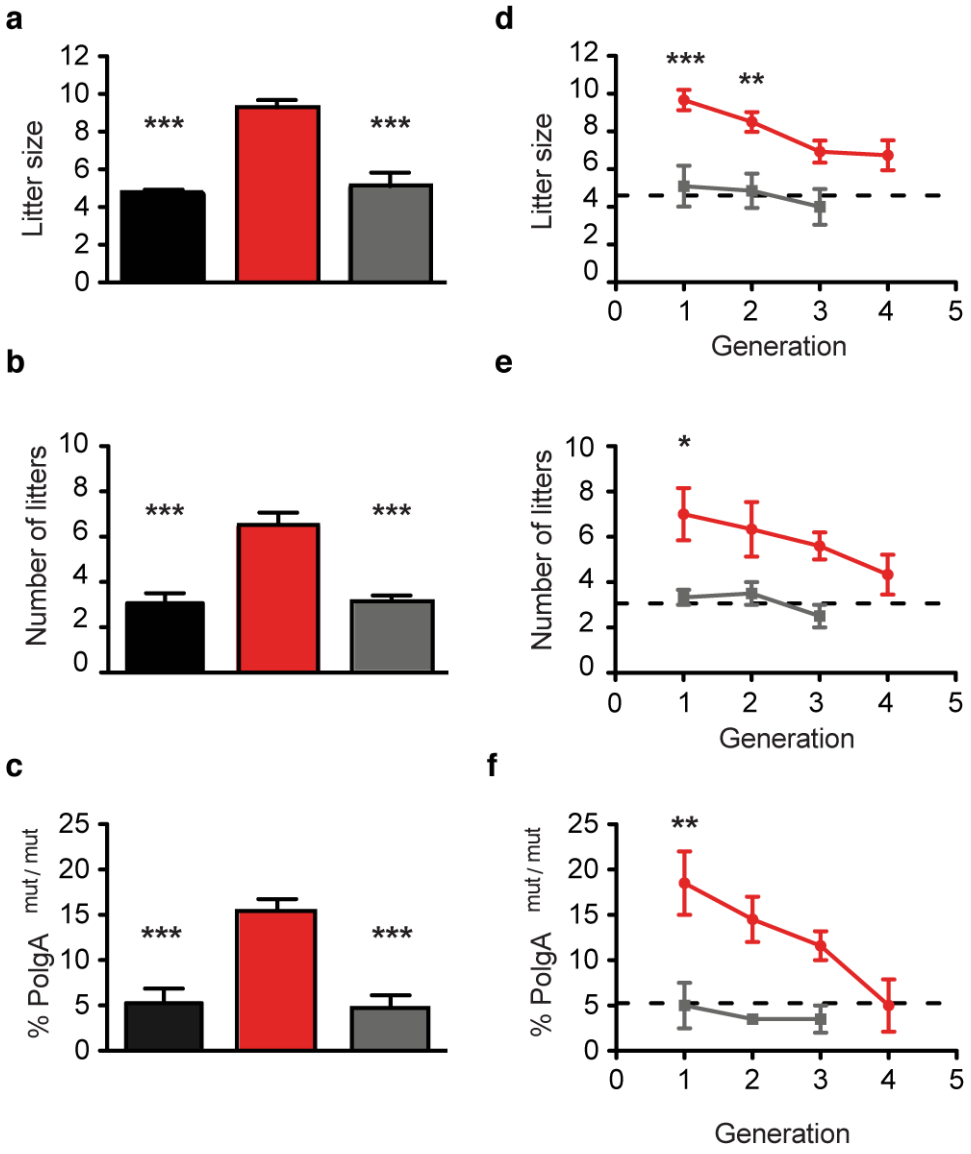

Figure 2. Anticipation of reduced fecundity obtained by intercrossing of heterozygous mtDNA mutator mice

a, Litter sizes from: standard intercrosses of *PolgA*$^{wt/mut}$ mice maintained by intercrosses for several generations (black bar, n=51), intercrosses of *PolgA*$^{wt/mut}$ mice after re-introduction of wild-type mtDNA into the females (red bar, n=42), intercrosses of *PolgA*$^{wt/mut}$ mice obtained by crossing wild-type males to heterozygous *PolgA*$^{wt/mut}$ females (grey bars, n=15). **b**, Number of litters per breeding pair. Crosses are as indicated in the legend to panel a. **c**, Proportion of live born *PolgA*$^{mut/mut}$ mice. Crosses are as indicated in the legend to panel a. **d**, Litter sizes after continuous intercrosses of *PolgA*$^{wt/mut}$ mice. The dashed line indicates the mean litter size of a standard intercross (n=51). The red line indicates an intercross where the mother in generation 1 contains re-introduced wild-type mtDNA. The mean litter sizes of *PolgA*$^{wt/mut}$ mothers belonging to generation 1–4 of this intercross are shown (n=21, 21, 15, 9, respectively). The grey line indicates an intercross where the *PolgA*$^{wt/mut}$ mice were obtained by crossing wild-type males to heterozygous mtDNA

mutator females. The mean litter size of mothers belonging to generation 1–3 of this intercross is shown (n=21, 9, 6, 9, respectively). **e**, Number of litters after continuous intercrosses of *PolgA*$^{wt/mut}$ mice. Crosses are as indicated in the legend to panel d. **f**, Proportion of live born *PolgA*$^{mut/mut}$ mice after continuous intercrosses of *PolgA*$^{wt/mut}$ mice. Crosses are as indicated in the legend to panel d. One-way ANOVA (panel a-c) and two-way ANOVA (panel d-f). *P<0.05, **P<0.01, ***P<0.001, Error bars = s.e.m.

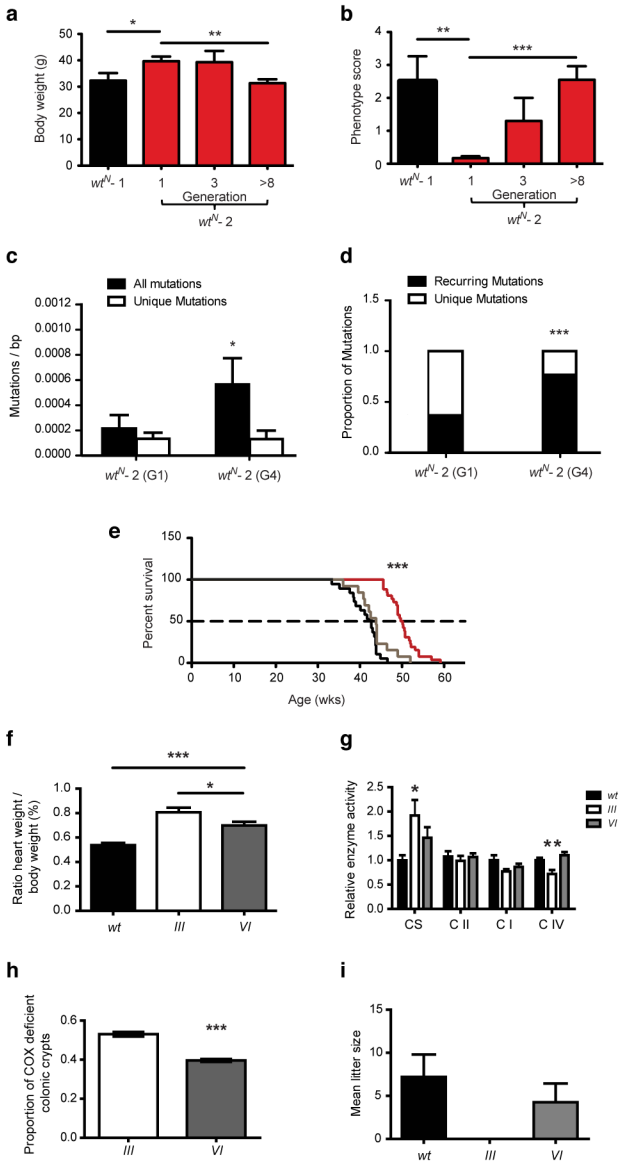

Figure 3. Premature ageing phenotypes in mice with a wild-type nuclear genome and in mtDNA mutator mice

a, Body weight at ~65 weeks in $wt^{N}-1$ (n=6) and $wt^{N}-2$ (generation 1 (G1) n=13, G3 n=5 and G>8 n=10). **b**, Phenotypic ageing score at ~65 weeks, $wt^{N}-1$ and $wt^{N}-2$ mice, Kruskal-Wallis or Mann-Whitney, post-hoc significances displayed. **c**, mtDNA mutation load comparisons of $wt^{N}-2$ G1 (n=6 animals) and G4 (n=3 animals). **d**, Proportions of unique and repeated mtDNA mutations of $wt^{N}-2$ animals from G1 and G4. Levels of clonally expanded point mutations increase from G1 to G4. **e**, Life span of $PolgA^{mut/mut}$ mice obtained from standard intercrosses of $PolgA^{wt/mut}$ mice (black line, n=19), intercrosses of $PolgA^{wt/mut}$ mice after re-introduction of wild-type (red line, n=26) and intercrosses of $PolgA^{wt/mut}$ mice obtained by crossing wild-type males to $PolgA^{wt/mut}$ females (grey line, n=13). Mantel-Cox test. **f**, The ratio of heart to body weight in 35–week-old wild-type mice (wt, n=10), *Type III* mice (n=9) and *Type VI* mice (n=9). T-tests with Welch's correction. **g**,

Respiratory chain function in heart at 35 weeks of age from wild-type mice (n=5), *Type III* mice (n=5) and *Type VI* mice (n=5). Relative enzyme activities of citrate synthase (CS), succinate dehydrogenase (CII), NADH dehydrogenase (CI) and cytochrome c oxidase (COX). Two-tailed, unpaired, t-tests. **h**, Proportion of COX-deficient colonic crypts at 35 weeks in *Type III* and *Type VI* mice. No COX-deficieny was present in age-matched controls (n=5 per genotype). **i**, Mean litter size after mating wild-type females to *Type III* males (n=8 matings) or to *Type VI* males (n=8 matings). The average litter size of wild-type (wt) mice is shown (black bar). One-way ANOVA (panel a,b), unpaired two-tailed t-test (panel c,f,g), Fisher's exact (panel d). **P*<0.05, ***P*<0.01, ****P*<0.001. Error bars = s.e.m (panels a,b,f,g,h), s.d. (panel c,i).

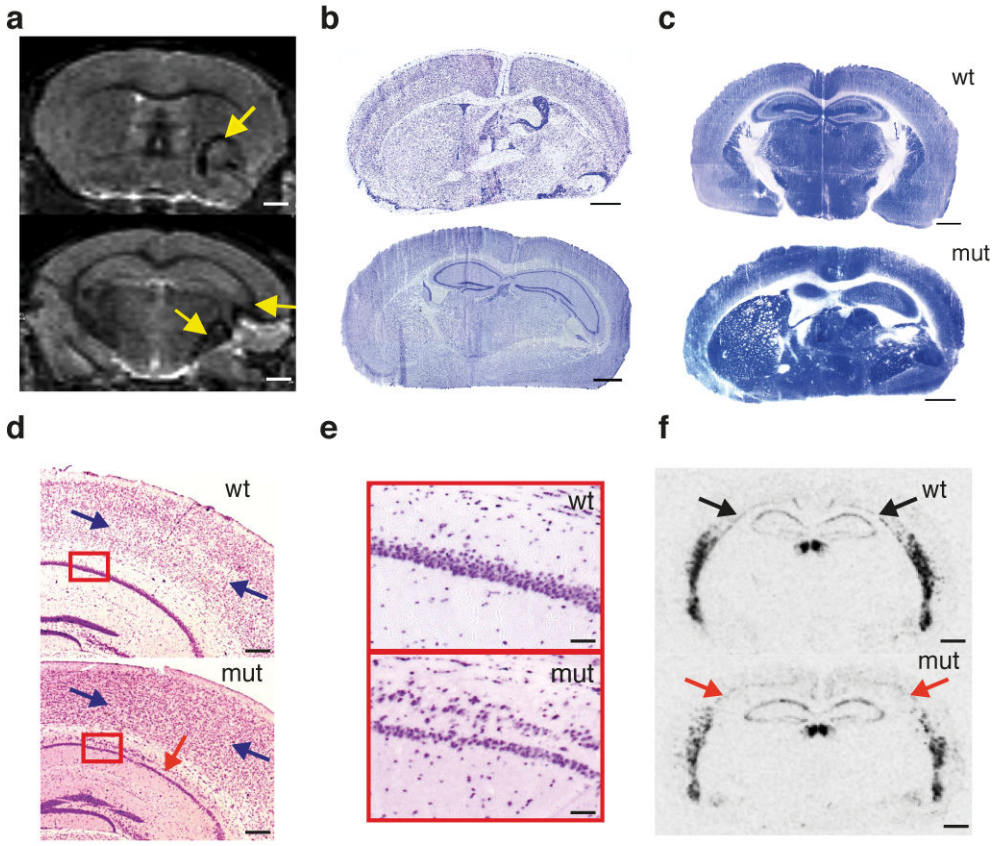

Figure 4. Focal and symmetric brain malformations in mtDNA mutator mice

a, MRI at two levels showing an abnormal signal from white matter in striatum (top panel) and elongation of the right hippocampal profile (bottom panel) in a 24 week old male mtDNA mutator mouse. **b**, Cresyl violet staining of brain sections at two levels showing severe striatal perturbations (top panel) and malformation of hippocampus (bottom panel) in the same mouse as the one depicted in panel a. **c**, Succinate dehydrogenase staining of brain sections of a wild-type (wt) and the mtDNA mutator mouse (mut) depicted in panel a. **d**, Cresyl violet staining showing cortical and hippocampal lamination disturbances, primarily affecting layers III-IV in cerebral cortex and CA1 pyramidal cells in hippocampus, in a 12 week old female mtDNA mutator mouse (mut). Analysis of an age-matched wild-type (wt) mouse is also shown. **e**, Increased magnification of boxed areas in panel d, showing hippocampal lamination disturbances in the mtDNA mutator mouse. Strikingly, stratum pyramidale is separated into two layers, with hippocampal pyramidal cells localized both in an outer, thin, less orderly layer and an inner, thicker, more orderly layer (lower panel). Analysis of an age-matched wild-type (wt) mouse is also shown. **f**, In situ hybridization to detect nuclear receptor related 1 (Nurr1) mRNA in the mtDNA mutator (mut) mouse depicted in panel d. Nurr1 expressing neurons are found in layers III-IV of the mtDNA mutator mouse (lower panel), contrasting with the normal expression pattern in layers V-VI (upper panel). Scale bars: 1 mm (panels a, b, c and f), 500μm (panel d), 125μm (panel e). Arrows indicate malformations in mtDNA mutator brain.